

Transition Region Blinkers I: Quiet-Sun Properties

D. Bewsher (danielle@mcs.st-and.ac.uk) and C.E. Parnell
*Mathematical Institute, University of St Andrews, North Haugh, St Andrews,
KY16 9SS*

R.A. Harrison
*Space Science Department, Rutherford Appleton Laboratory, Chilton, Didcot,
Oxfordshire, OX11 0QX*

Abstract. An automated method of identifying transition region blinkers is presented. The distribution and general properties of blinkers identified in the quiet Sun are discussed. The blinkers are seen most clearly in the O V transition region line, but they also have strong signatures in O IV, and the chromospheric line, He I. The strongest O V blinkers can also be identified in O III. No significant signatures are found for the blinkers in the coronal lines Mg IX and Mg X.

A few hundred O V blinkers are analysed. Their global frequency is between 1 s^{-1} and 20 s^{-1} depending on how significant the peaks of the blinkers are. They have a typical area of $3 \times 10^7 \text{ km}^2$, a typical lifetime of 16 minutes and a typical intensity enhancement factor of 1.8. We find the ratios of the oxygen lines to be flat confirming the result that blinkers are not temperature events, but are density enhancements or due to increases in filling factor. Blinkers are found to occur preferentially over regions of enhanced chromospheric or transition region emission such as network boundaries, however, it is not so clear that they appear below the brightest coronal regions. A rough analysis of the magnetic fragments show that blinkers preferentially occur above regions where there are large or strong magnetic fragments with 75% occurring in regions where one polarity dominates.

1. Introduction

Transition region blinkers are small-scale bright intensity enhancements and were first observed by Harrison (1997) using the Coronal Diagnostic Spectrometer (CDS; Harrison et al., 1995) which is onboard the Solar and Heliospheric Observatory (SOHO). They are most readily identified in O V, but are also found in other EUV lines, such as O IV, O III, He I and He II (Harrison, 1997, Harrison et al., 1999 and Berghmans et al., 1998). The properties of blinkers were investigated by Harrison (1997) and Harrison et al. (1999) who found that blinkers occur in quiet regions and (i) typically last between 1 and 40 minutes (average 17 minutes), (ii) have areas between $2 - 5 \times 10^7 \text{ km}^2$ and (iii) have intensity enhancement factors of 1.5 for the O V and O IV lines and 1.3 for O III. Ratios of the O V, O IV and O III intensity lightcurves of blinkers were studied to determine whether blinkers are density enhancements or temperature dependent features. These ratios were found to be flat.



© 2001 Kluwer Academic Publishers. Printed in the Netherlands.

Hence, blinker intensity enhancements were interpreted as being due to density or filling factor increases rather than a temperature increase. Harrison et al. (1999) studied just 97 events and found the global birth rate of blinkers to be just 1.2 s^{-1} .

Blinkers have also been identified using He II images taken from EIT/SOHO (Berghmans et al., 1998). Here the variation in properties of the events was larger with lifetimes, areas and intensity enhancement factors found between 2 – 60 minutes, $4 - 40 \times 10^7 \text{ km}^2$ and 1.1 – 2.7, respectively. They also found the global birth rate of He II blinkers to be between $0.3 - 20 \text{ s}^{-1}$ depending on the significance of the event peaks, although they suggest it might possibly be as high as 40 s^{-1} .

More recently, Brković et al. (2001) have analysed quiet-sun network and internetwork region movies taken by CDS in the He I, O V and Mg IX lines. From their results the typical area of a transition-region brightening is $2.4 \times 10^7 \text{ km}^2$ and the typical lifetime is 16 minutes. Like Berghmans et al. (1998) they also find a larger global frequency of 22 s^{-1} . Gallagher et al. (1999) using CDS noted some evidence for periodic behaviour of transient brightenings in the quiet sun network. They concluded that these brightenings were produced via rapid compression of the transition region plasma.

Chae et al. (2000) compare both SUMER and CDS data. They do not try to identify blinkers as such in the CDS data but rather focus on two regions that appear to have a blinker-like behaviour. In these regions many small-scale ‘unit brightening events’ are observed in the SUMER data with a size of a few arcsecs and a lifetime of a few minutes. Chae et al. (2000) report that these events are unlike explosive events since their UV line profile is not as broad, but they do still have significantly enhanced wings. Recently, Teriaca et al. (2001) also used SUMER to investigate the characteristics of such unit brightening events. They found that unit brightenings have a duration of just 200 s (< 4 minutes), their line profile has a slightly broadening and a -5 km s^{-1} blue shift. These events were also found to have no substantial variation in density about 10^{10} cm^{-3} in the O IV line. Hence, they suggest that an increase in filling factor is the most likely cause of the intensity enhancement.

All the initial results of blinkers (Harrison, 1997; Harrison et al., 1999) were carried out using manual detection and analysis techniques. We attempt to repeat this analysis here by using a more robust detection method in the hope of finding more events, as the results of Berghmans et al. (1998) and Brković et al. (2001) seem to suggest there should be. To do this we have developed an automated blinker identification routine (BLIP). Having identified the blinkers and their typical characteristics using BLIP we will use this information to compare the

locations of blinkers with the underlying magnetic field to investigate the magnetic structures below the blinkers. Other wavelengths (chromospheric, transition region and coronal) are also considered to see if blinkers have a typical signature in these lines. This work is described in the following sections: first we discuss the data set investigated (Section 2) before detailing the algorithm used to detect and analyse the blinkers (Section 3). In Section 4 the results are presented. The conclusions drawn from these results are detailed in Section 5.

2. Data

In this paper we use data taken by two SOHO instruments: CDS and MDI. The CDS dataset is taken using the normal incidence spectrometer (NIS), which has wavelength ranges of 308-381Å and 513-633Å and enables the solar atmosphere to be observed at a wide range of temperatures, from the chromosphere, through the transition region and into the corona. The data sequence was taken using the $4'' \times 240''$ slit, but only the central $124''$ were telemetered, hence the slit rasters have an area of $40'' \times 124''$. The exposure time at each slit location is 10 seconds and the entire raster has a duration of 151 seconds. Each pixel is $4''$ in the solar-x direction and $1.7''$ in the solar-y direction, producing rasters of size 10×73 pixels. The data contains 6 emission lines, He I 584Å, O III 599Å, O IV 554Å, O V 629Å, Mg IX 368Å and Mg X 624Å formed at the respective temperatures of 20,000 K, 100,000 K, 160,000 K, 250,000 K, 1,000,000 K and 1,200,000 K.

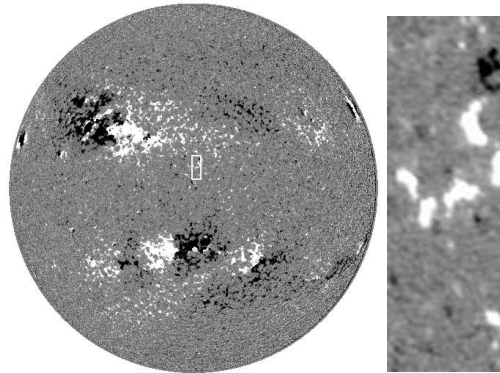


Figure 1. Full disk MDI magnetogram taken on 29th November 1998 at 12:48 UT. The white box indicates the area covered by the CDS rasters investigated. Partial frame high resolution MDI magnetogram showing the magnetic field below the CDS raster.

The data sequence analysed (S15251) was taken on 29th November 1998 and lies over a region of quiet sun as can be seen in Figure 1.

The start of the observation run was 11:27 UT and it lasted almost 12 hours; there were 270 rasters. The coordinates of the centre of the first raster are 4.80" W and 111.50" N. The observations are feature tracked by the movement of the mirror until it has reached its maximum offset and then by the movement of the legs so the mirror can once more scan its full range.

The standard CDS software is used to correct the data for missing pixels, CCD readout bias and cosmic ray hits, flat fielding effects and finally a calibration is used to convert the data units to photons-events per pixel per second (p/p/s). The tilt between the NIS dispersion axis and the CCD detector is corrected for, however, the standard correction is not applied because it has been found that the tilt is dependent on time and mirror position (Bewsher et al., 2001). The rotation effect of the Sun is removed from the data by using ROTXY from solarsoft. All images are rotated back to the first image which is used as a reference point. Since the CDS pixels are several arcsecs in the x-direction many of the images are rotated back by some fraction of a pixel. We use bilinear cubic interpolation to achieve this sub pixel rotation.

The MDI data used is from the high resolution field of view and has a cadence of 1 minute and pixels of size 0.6" × 0.6". We group the data into sets of 3 consecutive images and average these, thus reducing the cadence of the data to that of the CDS images, as well as reducing the noise in the MDI data.

3. BLinker Identification Program (BLIP)

In order to objectively detect blinkers, we designed a BLinker Identification Program (BLIP) which is an automated method of finding blinkers from a series of CDS rastered, feature tracking data. The algorithm finds groups of pixels that have 'significant' simultaneous peaks.

In order to determine if a peak is significant we first calculate the statistical error of each pixel using the method described in Thompson (1998), where the statistical noise is given by,

$$f_N = \sqrt{\frac{2}{N}} \quad (1)$$

where N is the number of photon-events/pixel. The noise must be calculated in this way because the 4 dimensional CDS data has been reduced to 3 dimensions by simply summing up the spectral data in each pixel rather than fitting a line to it. For each data series and each particular wavelength an error threshold (λ) is then determined; λ is defined as the value below which 99% of the errors exist.

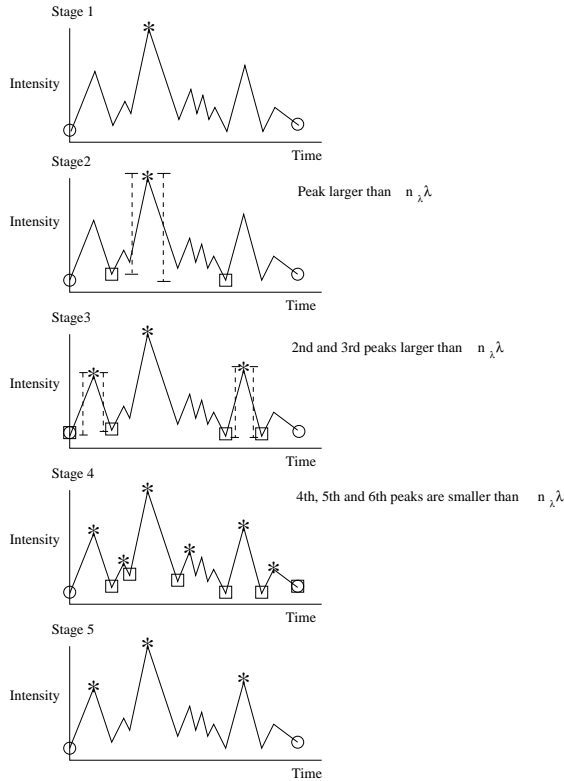


Figure 2. Illustration of how significant peaks are chosen in BLIP. The peaks investigated are denoted by an * which remains if the peak is significant. The \square s denote the minimum troughs either side of the peaks investigated.

For each pixel in the data array all the local temporal maxima and minima (peaks and troughs) are identified. Clearly, not all peaks are going to be associated with a blinker. We only keep peaks that are larger than $n_\lambda \lambda$, where n_λ is a positive integer that is specified later. To determine each pixel's significant temporal peaks, the largest peak in each pixel's time series is taken and the difference between it and the minimum trough both before and after is calculated. If the value of the intensity jump between the peaks and troughs is larger than the threshold, $n_\lambda \lambda$, then the peak is kept and the process repeated for the time interval before and after the maximum peak. If the difference in intensity is less than $n_\lambda \lambda$, then the peak is neglected and that section of the time series is investigated no further. Figure 2 shows a schematic of how this procedure works. In this intensity-time sequence three significant peaks are found.

Adjacent pixels that peak in the same image are grouped together to form an event. A pixel is said to be adjacent to another if it is one

of the 8 surrounding pixels. A group must have at least n_p pixels to be counted as an event, where n_p is a positive-integer that is specified later.

A check is then made to see if each event is actually a blinker by testing to see if it still meets the criteria for a blinker, i.e. its peaks and troughs are identified and compared in the same way as above. If a peak is identified in the group intensity profile at the same raster as the original peak used to group the pixels and this peak is still greater than $n_\lambda \lambda$ above the troughs, then the group is counted as a blinker. This step is necessary because it is possible that the sum of the pixel intensities may smooth out any peak if some of the troughs about the peak are widely separated in the different pixels that make up the group.

Having found all the blinkers, their properties can then be determined. Area, lifetime, intensity enhancement factor and global frequency are all calculated from the intensity curves and the number of events can also be determined.

4. Results

4.1. PROPERTIES OF BLINKERS

We use BLIP to investigate a series of different sizes of blinkers by varying the minimum size, n_p , and minimum intensity jump factor, n_λ , in each run of our algorithm. The following combinations of n_p and n_λ were considered: $n_p = 1, 2$ or 3 CDS pixels and $n_\lambda = 5$; and $n_p = 3$ and $n_\lambda = 3$ or 10. The error threshold, λ , for the O V data equals 3.64 pps. Table I shows the numbers and properties of the blinkers identified.

Table I. Properties of the quiet-sun blinkers identified using BLIP

Properties	n_λ	3	5	5	5	10
	n_p	3	1	2	3	3
No. of blinkers		356	214	171	136	17
Global frequency (s^{-1})		19.5	11.7	9.4	7.5	0.9
Mean intensity enhancement factor		1.7	1.7	1.8	1.8	2.1
Mean area ($\times 10^7 \text{ km}^2$)		3.1	2.0	2.5	2.9	2.9
Mean lifetime (minutes)		16.4	16.4	16.4	16.4	21.0
Mean rise time (minutes)		8.1	8.3	8.2	8.2	10.6
Mean fall time (minutes)		8.3	8.2	8.2	8.2	10.3

The mean areas and mean lifetimes determined for the blinkers are found to be comparable with those found by Harrison et al. (1999). Furthermore they do not vary greatly with a change in the parameters, n_λ and n_p . The maximum area of a blinker is found to be $5.5 \times 10^8 \text{ km}^2$, and the minimum area is restricted by the choice of n_p and equals $3.6 n_p \times 10^6 \text{ km}^2$.

The mean lifetime of the blinkers identified with each criterion is about 16.5 minutes. The longest blinkers are identified with $n_\lambda = 3$ and $n_p = 3$ and have a lifetime of order 40 minutes. The shortest blinkers are identified with $n_\lambda = 3$ and $n_\lambda = 5$ and have lifetimes of the order of 6 minutes. This lower limit is instrumental and is simply the shortest observable blinker time with our data set.

The mean rise and fall times of the blinkers appears to be equal, however, on closer inspection, we see that this does not mean that in each blinker the rise time equals the fall time. In all cases, except $n_\lambda = 10$ and $n_p = 3$, the numbers of blinkers with rise time greater than fall time and fall time greater than rise time is approximately 40%, but there are a larger number of events with a greater rise time. In just 20% of cases the rise and fall time are approximately equal. In the $n_\lambda = 10$ and $n_p = 3$ case we find that there are more blinkers (45%) with fall time greater than rise time, but still approximately 20% of cases have almost equal rise and fall time.

The intensity enhancement factors are higher than those observed by Harrison et al. (1999). The reason for this is not clear, although it may be due to a difference in the way the lower intensity bound is determined. We consider the change from the troughs on either side whilst Harrison et al. (1999) estimate the change from an average minimum intensity.

Not surprisingly, we find a much greater global frequency than Harrison et al. (1999); the global frequency is defined as the number of blinkers that occur on the whole sun per second assuming that our CDS field of view is representative of the whole sun. This is most likely to be because manual detection is a difficult and time consuming process and is rarely as successful as automated detection, especially for blinkers with small intensity enhancement factors. In the case where n_λ is held fixed and n_p decreases from 3 to 2 and from 2 to 1 we see 25% more blinkers identified each time. Similarly, when n_p is held fixed at 3 and n_λ is decreased from 10 to 5 and from 5 to 3 we find 800% and 240% more blinkers, respectively. These increases are not too surprising since we are allowing smaller events to be counted as blinkers each time. We feel that an intensity jump factor around 3 or 5 is probably a reasonable value. Any lower value would involve many fluctuations due to noise being counted as blinkers. Similarly it is preferable to have a blinker

detected in more than one pixel, however, here we have to bear in mind that the CDS pixels are fairly large and so an instrument with higher spatial resolution would be desirable to estimate more reliably the sizes and numbers of blinkers.

4.2. INTENSITY PROFILES

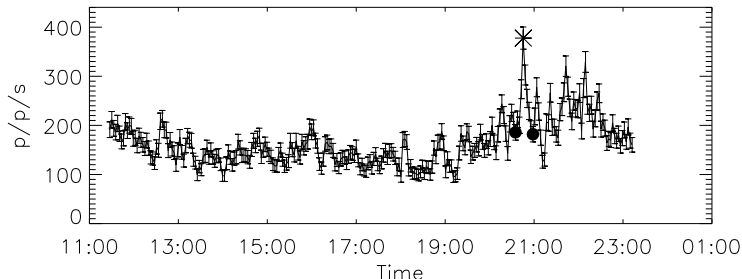


Figure 3. A typical O V blinker identified with $n_\lambda = 5$ and $n_p = 3$. The * shows the peak, and the dots mark the start and end of the blinker.

In Figure 3, the intensity of a typical O V blinker is plotted against time. The peak of the blinker (*) and the beginning and end of the blinker (dots) are marked. The statistical error of the intensity calculated using Equation 1 is also plotted. Due to the large number of data points on this graph the profile of the blinker is hard to distinguish - Figure 4 shows a close up of the blinker.

Looking at all the blinker lightcurves we see that there appear to be two types of blinker activity. The first is repetitive in nature - the same group of pixels peak more than once during the observing period - and the second show no recurrence. Approximately 75% of blinkers studied display a repetitive nature, with just 25% of blinkers having one single peak during the observing period. The high percentage of repetitive brightening is suggestive that the mechanism that causes blinkers is not an irreversible process such as reconnection but rather a more subtle process that can switch off and on. Harrison et al. (1999) finds that there is a 50% chance of a blinker onset on the same site within 3000s (50 mins). It is possible that there may be some sort of periodicity to the repetition of peaks in the blinker lightcurves. To test this hypothesis we analysed the blinker lightcurves using Fourier analysis. Our analysis revealed no sign of any periodicity or oscillatory behaviour. This may be because the recurrence rate of blinkers is on the order of several hours, rather than the hour suggested by Harrison et al. (1999) and our 12 hour data sets are not long enough to show

these. We also attempted some wavelet analysis to see if the blinkers appeared in groups, but again we saw no sign of any distinct wave packets.

4.3. BLINKER SIGNATURES IN OTHER WAVELENGTHS

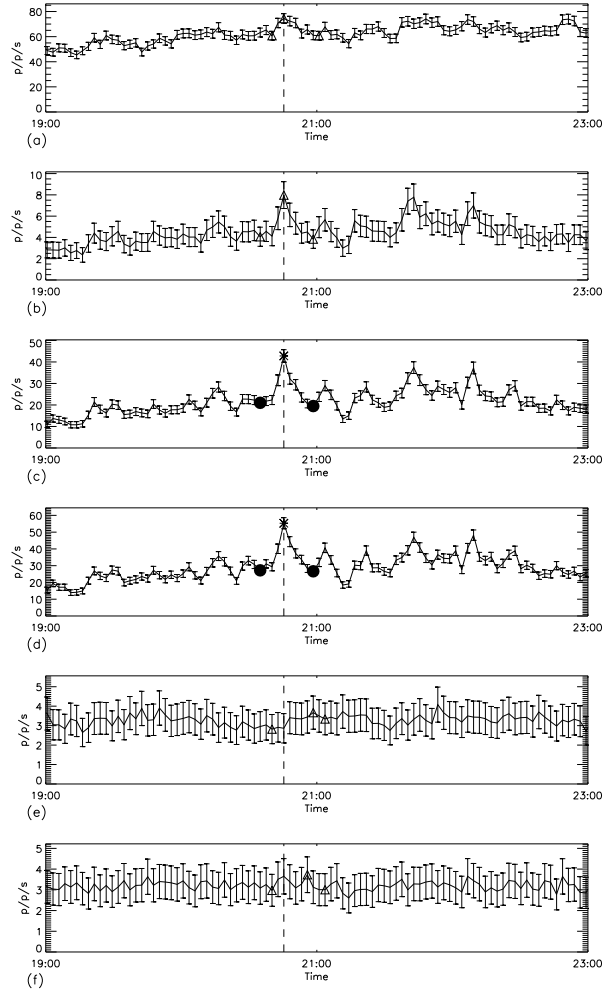


Figure 4. Comparison of intensity lightcurves for a blinker identified in O V seen in different wavelengths, (a) He I, (b) O III, (c) O IV, (d) O V, (e) Mg IX, and (f) Mg X. The * mark the peaks of identified blinkers, and the dots mark the starts and ends of the blinkers. The Δ s mark the start, peak and end of all enhancements found by BLIP that are not large enough to be blinkers. The dashed line indicates the peak of the O V blinker.

In Figure 4, the lightcurves relating to the same group of pixels as shown in Figure 3 are plotted against time for He I, O III, O IV, O V, Mg IX and Mg X (a-f respectively). Each lightcurve is investigated to determine whether it has a peak at the right time that satisfies the criteria for a blinker. An enhancement in intensity can be seen in the He I, O III, O IV and O V lines. However, the only one of these events, apart from the O V, to meet the criteria for a blinker is the O IV peak. The blinker identified in O IV starts, peaks and ends at the same time as the O V blinker. Even though a blinker is not registered in the OIII line, there is a noticeable ($n_{\lambda\text{OIII}} = 2.8$) increase in intensity which starts, peaks and ends at the same time as the other O line blinkers. There is also a notable ($n_{\lambda\text{HeI}} = 2.6$) increase in intensity in the He I line. These are identified by Δ s.

The blinker picture in Figure 4 is similar to that seen in about 25% of the blinkers identified. Table II shows the numbers of blinkers observed first in O V and then in one, two or three other wavelengths. In all cases, 80-91% of the O V blinkers were also identified in the O IV line; this confirms the results by Harrison et al. (1995) that the blinkers are most evident in the O V and O IV transition region lines. The majority of these blinkers are also identified in He I. Indeed, in all cases, except one ($n_{\lambda} = 10$ and $n_p = 3$), 23-28% of blinkers identified in O V are also identified in the He I and O IV. In the $n_{\lambda} = 10$ and $n_p = 3$ case only 6% of blinkers are identified in these three wavelengths. In all cases, less than 6% of O V blinkers were seen in the O III line. These blinkers are generally the strong blinkers and are also visible in the O IV and He I. No blinkers were identified in either of the hotter coronal magnesium lines. The reason blinkers have not been identified in the O III and the coronal lines may be because these lines are weak in quiet regions.

To establish the size of the intensity enhancements identified in the other wavelengths at the same time as the blinker in O V we calculated the size of the peaks in the same way as we tested to see if the peaks were blinkers. Table III shows the range of the sizes of peaks in terms of their peak-size factors even if this factor is less than that required for a blinker. The results shown are only for the events associated with blinkers seen in O V and with $n_{\lambda} = 5$ and $n_p = 3$.

The results in this table show that the peaks identified in the coronal (magnesium) lines are much smaller than that required for a blinker, with just 3.7% and 13.2%, respectively, for the Mg IX and Mg X having peak factors greater than 1. The largest O III peak is only just significant enough to be counted as a blinker, with a peak factor of 5.4. In the other O lines (O IV and O V) and the He I line the majority (99%, 100% and 49%, respectively) of peak factors are above 3. The maximum peak factors of the blinkers in these wavelengths are

Table II. Number of events identified as blinkers in O V and other wavelengths

Wavelength	n_λ	3	5	5	5	10
	n_p	3	1	2	3	3
O V		356	214	171	136	17
He I/O V		104	58	46	37	1
O III/O V		23	3	3	2	0
O IV/O V		323	171	143	118	14
Mg IX/O V		0	0	0	0	0
Mg X/O V		0	0	0	0	0
He I/O IV/O V		99	50	40	34	1
He I/O III/O V		17	3	3	2	0
O III/O IV/O V		23	3	3	2	0
He I/O III/O IV/O V		17	3	3	2	0

Table III. Range of peak-size factors for events in all wavelengths first identified as O V blinkers with $n_\lambda = 5$ and $n_p = 3$

Wavelength	λ	Minimum peak factor	Maximum peak factor	% w. peak factor > 1	% w. peak factor > 3
He I	5.35	0.0	12.4	89.7	47.8
O III	1.40	0.3	5.4	94.1	21.3
O IV	3.16	2.3	13.1	100.0	99.3
O V	3.64	5.1	12.4	100.0	100.0
Mg IX	1.15	0.0	1.4	3.7	0.0
Mg X	1.05	0.0	1.8	13.2	0.0

not a lot bigger than 10, confirming our thoughts that an $n_\lambda = 10$ just identifies the very large blinkers. It is possible that the events in the Mg X line appear much larger than in Mg IX because the Mg X line also includes an O IV component.

4.4. LINE RATIOS

Figure 5 (a) shows the lightcurve seen in Figure 3 whilst Figures 5 (b-d) show its ratio with the He I, O III and O IV lightcurves, respectively. The dashed line marks the position of the peak of the O V blinker in all

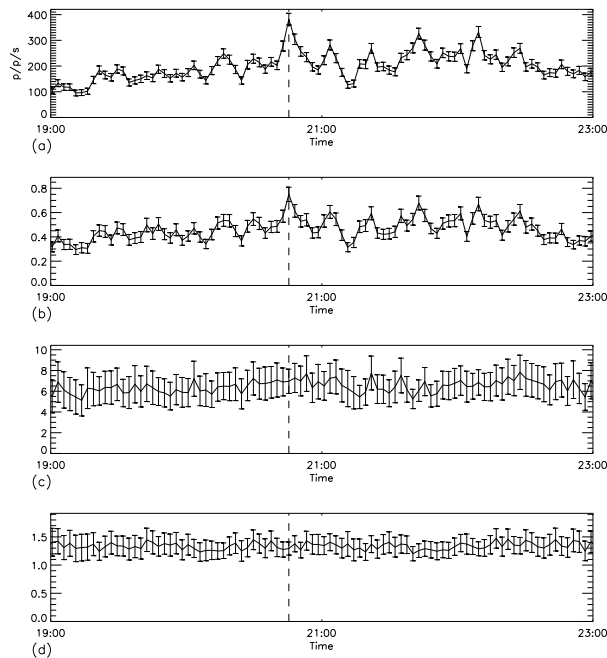


Figure 5. (a) Typical O V light curve, (b) Ratio of O V/He I, (c) O V/O III and (d) O V/O IV. The dashed line indicates the peak of the O V blinker.

figures. The ratio of the oxygen lines show no significant temporal variations. This is similar to the result found by Harrison et al. (1999) and suggests that blinkers are not temperature enhancements, but rather enhancements in density or filling factor.

We considered, for all our blinkers, the minimum, mean and maximum values of the line ratios of the lightcurves calculated between the start and end of the O V blinker, as well as for the entire ratio of the lightcurves (Table IV). It appears in all cases as if the blinker part of the lightcurve ratio is slightly bigger than that normally observed, except for the ratio of O V/O IV where the blinker ratio is slightly lower than expected. If these deviations were real it would imply that the typical temperature of a blinker lay somewhere between 10^5 K and 1.6×10^5 K, however, the typical 1σ error on these ratios is 1.32 and 0.17 for the O V/O III and O V/O IV ratios, respectively. Since the differences between the mean values of the blinker and entire lightcurves are always less than these errors it is unlikely that the differences are real, hence, we conclude that the ratios of the oxygen species are effectively flat and so agree with the results of Harrison et al. (1999).

Table IV. Minimum, mean and maximum line ratio values for the entire lightcurve and for the blinker region only

Wavelength	Minimum		Mean		Maximum	
	Entire	Blinker	Entire	Blinker	Entire	Blinker
He I	0.26	0.32	0.42	0.48	0.54	0.93
O III	3.93	4.77	6.26	6.38	7.22	7.74
O IV	1.14	0.99	1.32	1.29	1.59	1.57
Mg IX	3.06	5.13	9.97	11.97	15.66	19.53
Mg X	3.38	6.04	10.16	11.97	13.94	18.85

4.5. RELATIONSHIP TO NETWORK

To compare the location of the blinkers with the network and the emission from other wavelengths we plot the integrated emission over the entire observing sequence of the derotated He I, O III, O IV, O V, Mg IX and Mg X rasters, Figure 6 (a-f), respectively. The Δ 's represent the location of the midpoints of the blinkers, and the * in the top right-hand corner shows the midpoint of the blinker that has been discussed in detail.

Clearly the blinkers are not distributed uniformly over the field-of-view. Indeed, just the odd one or two blinkers seem to appear off the network boundary. To see if the blinkers are distributed uniformly with respect to intensity, which from the images they clearly appear not to be, we use a likelihood statistical test. First we determine the numbers of pixels with intensities in certain ranges. These ranges (bins), of which there are k , are chosen such that the width of the bin increases by a factor of 2 for increasing intensity. We define M to be the total number of pixels and M_i to represent the numbers of pixels in the i th range. Similarly, n represents the total number of pixels associated with the peak of each blinker whilst n_i is the number of these pixels with intensities in the i th range. The likelihood ratio statistic, w_k , is then defined as

$$w_k = 2n_i \sum_{i=1}^k \log \left(\frac{n_i M}{n M_i} \right). \quad (2)$$

We can now compare w_k with the expected χ_{k-1}^2 statistic. If w is large compared to χ_{k-1}^2 then the distribution is not uniformly distributed and suggesting that they are dependent on brightness of emission.

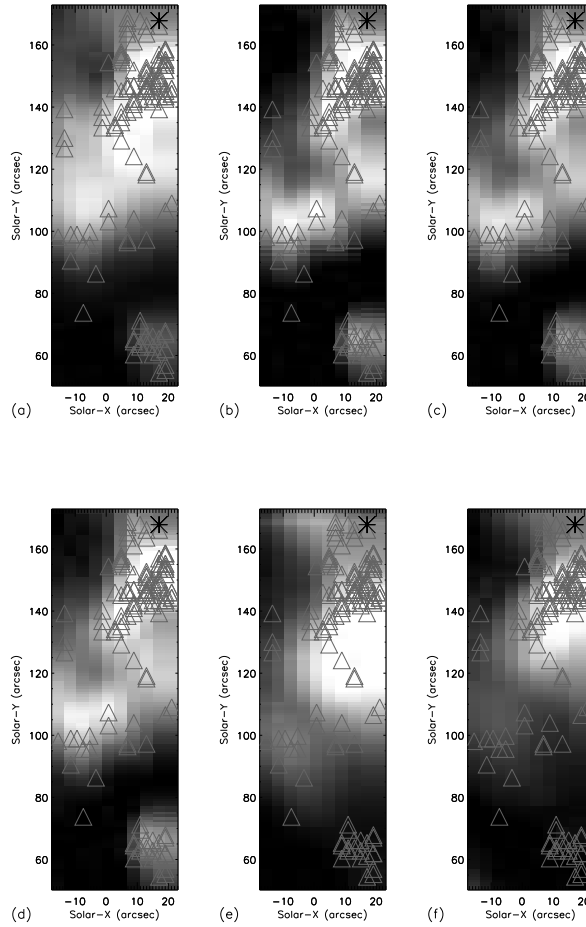


Figure 6. Comparison of the location of blinkers with the network. Time integrated emission of the derotated (a) He I, (b) O III, (c) O IV, (d) O V, (e) Mg IX and (f) Mg X rasters. Each Δ represents a blinker and the * refers to the blinker seen in Figure 3.

The results of this analysis for the $n_\lambda = 5$ and $n_p = 3$ case are shown in Table V. In all cases the likelihood ratio statistic is substantially (between 2 and 300 times) greater than the χ^2_{k-1} value, so clearly the blinkers are not uniformly distributed. This is no surprise for the O V blinkers, since by definition they are the brightest pixels, however, it is interesting that this still holds for the coronal lines even though we cannot detect blinkers there.

Table V. Values of the likelihood ratio statistic and corresponding χ^2_{k-1} statistic for blinker events identified with $n_\lambda = 5$ and $n_p = 3$.

Wavelength	k	χ^2_{k-1}	Likelihood ratio statistic
He I	4	17.73	795.622
O III	4	17.73	3129.42
O IV	6	22.11	4078.15
Mg IX	3	15.20	175.042
Mg X	3	15.20	957.243

In most cases the blinkers appear to occur above regions of enhanced emission. A further analysis is used to determine whether blinkers are located over the areas of strongest emission. Figure 7 shows the distribution of intensity of CDS pixels in all wavelengths and blinker pixels (identified with $n_\lambda = 5$ and $n_p = 3$) at the time of the blinker peak. The solid line shows the distribution of pixels associated with blinkers and the dashed line shows the distribution of all pixels. From Figure 7 we can see that in all wavelengths the pixels with the weakest emission are not associated with blinkers and in the cases of He I, O III, O IV and O V the blinkers are clearly associated with the top few percent of pixels with the highest intensity. This, as already said, is no surprise in the case of O V since, by definition, blinkers are the high emission pixels, however, since this pattern is mirrored in the other wavelengths it implies that blinkers probably generally have similar signatures in these other wavelengths too. Also it confirms the results that blinkers occur above the network in quiet regions. However, in the coronal lines the results are not quite the same. The blinkers do not appear to be associated with the high intensity pixels in the Mg IX line, although in Mg X they do appear to be. It is possible that the O IV component of the Mg X line may be confusing these results and that, if this test were repeated using fitting techniques to the spectra to reduce the data rather than just summing all spectral counts, then a clearer result may appear.

4.6. RELATIONSHIP TO MAGNETIC FIELD

The location of the blinkers can also be compared to the magnetic fragments in the photosphere below. In Figure 8 the location of the mid-point of the blinkers (Δ s) are drawn over sections of MDI magnetogram taken at three different times. Note, that the blinkers themselves are

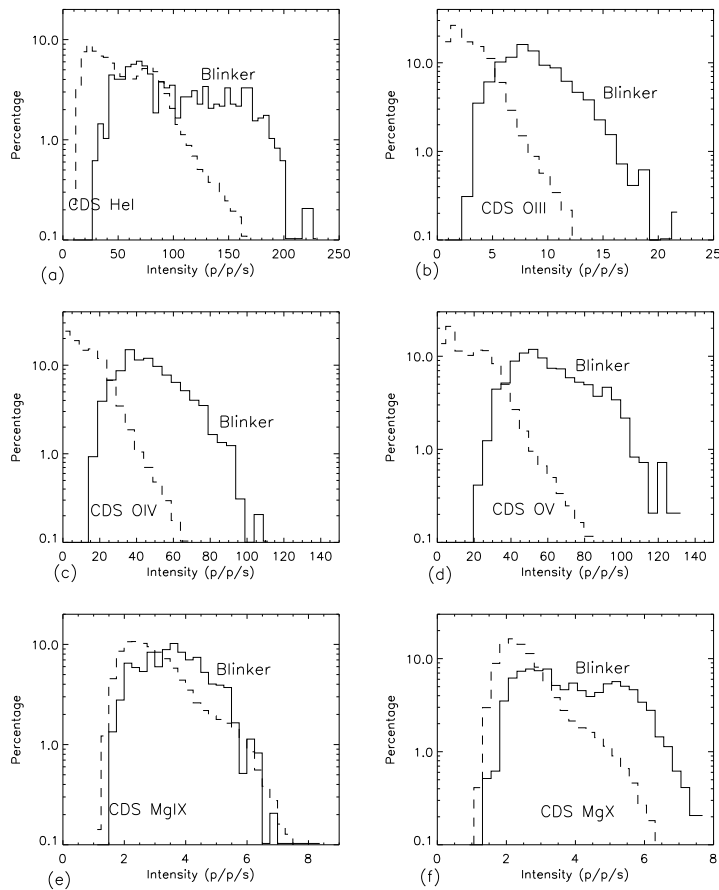


Figure 7. Histogram of distribution of all pixels intensities (dashed) and blinker pixel intensities (solid) for (a) He I, (b) O III, (c) O IV, (d) O V, (e) Mg IX and (f) Mg X lines respectively.

much bigger than the symbols shown. The Δ s over each magnetogram, going from left to right, are those that occur in the first 4 hrs 11 mins, the next 4 hrs and 32 mins and the final 2 hrs and 56 mins, respectively. The blinker shown in Figure 3 is marked with an * and the underlying MDI image is taken at 20:45, the nearest frame to the peak of this blinker. The \times s indicate the blinkers that peak at the same time as the other two magnetograms. Although, all the other blinkers are marked it is important to remember that they peak at different times and therefore the actual magnetic field below may have changed considerably.

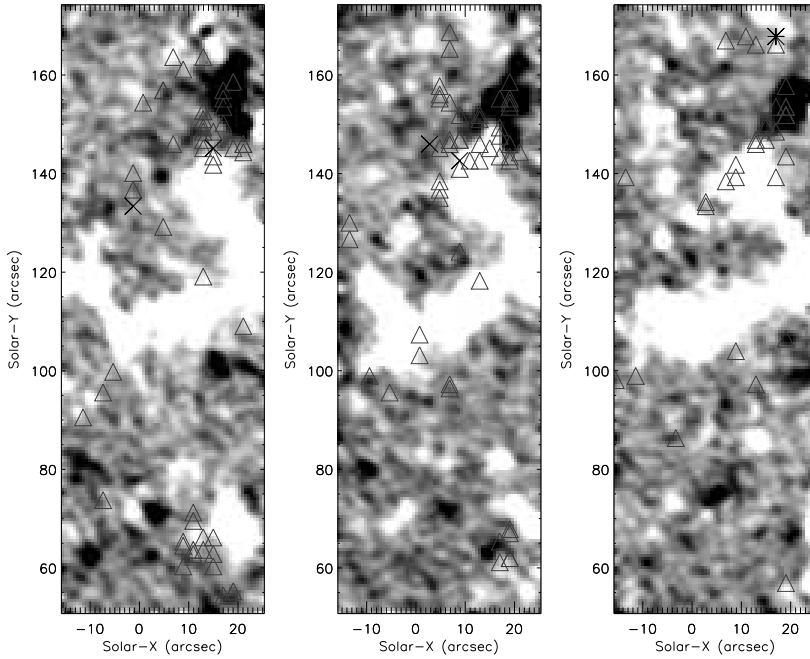


Figure 8. Comparison of the location the midpoints of the $n_\lambda = 5$ and $n_p = 3$ blinkers (Δ s) with the underlying magnetic field. Sections of MDI magnetograms, with maximum colour intensity limits set for absolute fields above 20 Mx cm^{-2} , are shown at times 14:10 (left), 18:16 (middle) and 20:45 (right). From left to right over each magnetogram there are, respectively, 51, 52 and 33 blinkers. The \times s indicate the blinkers that peak in the left and middle frames whilst the $*$ indicates the blinker which has been discussed in detail throughout this paper.

Consider the five blinkers that peak at the time of the images (shown by \times s and a $*$). Figure 9 shows a close up of these blinkers taken by CDS in the O V line, as well as the corresponding magnetic field below. The blinkers from left to right (a-e) are ordered as they are seen from left to right in Figure 8. The first blinker, Figure 9a, appears above a region where there are no fragments save a small, weak negative magnetic fragment to the right. The second, Figure 9b, occurs directly above a large negative fragment, although the blinker may just touch

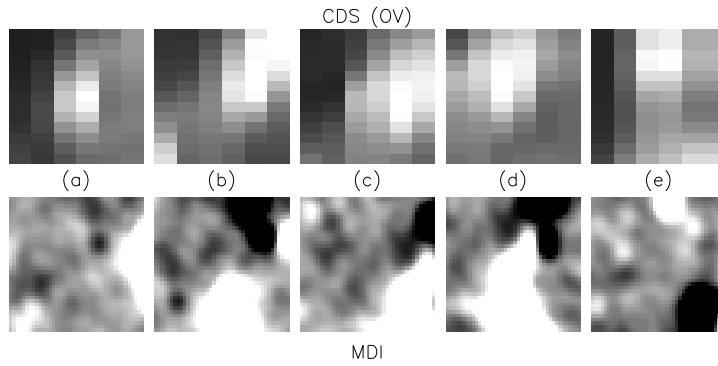


Figure 9. Images in the CDS O V line of the five blinkers indicated in Figure 8 by \times s and a *; (a-e) corresponds to their order from left to right as seen in Figure 8. The MDI images are of the magnetic field below the blinkers taken the time of the peak of each blinker; maximum colour intensity limits set for absolute fields above 20 Mx cm^{-2} .

the large positive fragment below. The blinker in Figure 9c is similar in that it is predominantly over the large positive fragment, but may just touch the large negative one nearby. In Figure 9d the blinker overlies large fragments of both polarities, whilst the last blinker, Figure 9e, just overlies the positive fragment at the top of the image.

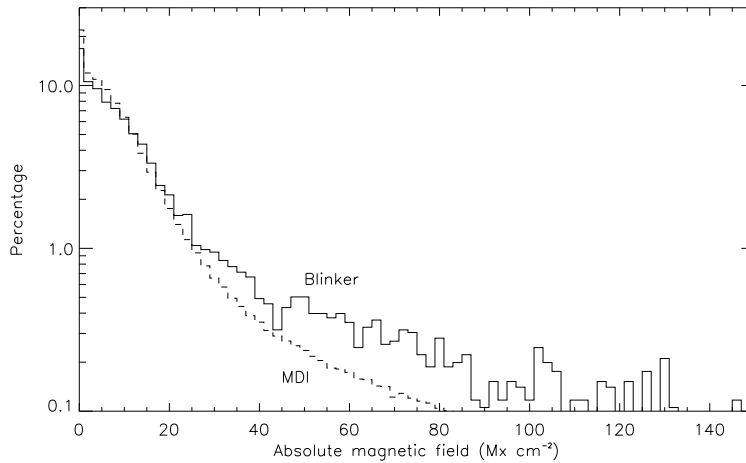


Figure 10. Distribution of blinker pixel values (solid) and all pixel values (dashed) versus absolute magnetic flux.

Clearly, from the illustration of these five blinkers we see that the nature of the magnetic fields below blinkers is not clear cut. All situations arise. Mixed magnetic fields directly below the blinker are not

essential, however, in most cases reasonable sized magnetic fragments of one polarity are found. In Figure 8 it appears as if a few blinkers occur in regions where there are no well defined fragments. A similar likelihood ratio test to that described in the previous section is performed to determine whether blinkers are preferentially occurring above regions of strong absolute magnetic field. Here the MDI pixels are binned into k bins according to their absolute field strength with, this time M representing the total number of MDI pixels, M_i the number of these pixels in each bin, n represents the total number of MDI pixels associated with the peak of each blinker and n_i the number of these pixels in each bin. The likelihood ratio statistic, w_k , is calculated in exactly the same way as before. We again find that w_k (which equals 580.5) is considerably larger than the χ_{k-1}^2 , (which equals just 27.9 for $k = 9$) and so the distribution of the blinkers above the magnetic field is not uniform. Furthermore, by comparing the distribution of blinker pixels (identified with $n_\lambda = 5$ and $n_p = 3$) and the absolute strength of the magnetic field (Figure 10) we see that blinkers do generally occur above the pixels with stronger absolute field strength. However, as we have already seen, blinkers can also occur above all field strengths and are not just confined to strong fields. This may be because, the actual roots of the fieldlines involved in the blinker have strong field, but are confined in rather small areas, whereas due to the canopy effect (Gabriel, 1976) the blinker itself may spread over a much wider area.

Table VI. Numbers and polarities of magnetic fragments below the $n_\lambda = 5$ and $n_p = 3$ blinkers

Polarity	Number (Size - in MDI pixels) of Magnetic Fragments		
	One (> 10)	Two: one (> 10) of major sign one (< 10) of opposite sign	One (< 10)
Positive	35	34	6
Negative	11	15	1
Positive+Negative	25	-	9

As a crude estimate of the types of magnetic fragments that lie below blinkers we counted the numbers of pixels below each blinker that had less than -10 Mx cm^{-2} and above 10 Mx cm^{-2} . If there were less than 10 MDI pixels of one polarity we counted that as a small fragment and if there were more than 10 MDI pixels of one polarity we counted that as a large fragment. Table VI indicates the numbers of fragments below the $n_\lambda = 5$ and $n_p = 3$ blinkers.

Clearly most (88%) blinkers occur above large fragments of one or both polarities. Furthermore 75% occur above regions where one polarity dominates. This suggests that it is the presence of large or strong magnetic regions that is important for blinkers rather than close pairs of opposite polarity magnetic fragments. It is interesting that 51% of blinkers occur above regions where large positive fragments dominate, whereas only 19% occur above regions where negative fragments dominate. This is probably because our CDS rasters have only a fairly small field of view and are situated above regions of network field that are dominated by positive magnetic fields.

5. Discussion

The most important question to ask is ‘What mechanism gives rise to blinkers?’ Before we can answer this we must compare our results with those of other events.

First, let us compare rates of occurrence of blinkers with rates of occurrence of events that occur in the photosphere near network regions. The most obvious of these to consider is the rate of emergence of ephemeral regions which has recently been revised by Hagenaar (2001) and is now about $8.4 \times 10^{-24} \text{ cm}^{-2} \text{ s}^{-1}$ or in other words, just less than one per supergranule (radius: 7,000 km, geometry: hexagonal, area: $3\sqrt{3}r^2/2 \approx 1.3 \times 10^8 \text{ km}^2$) per day. Cancelling magnetic features are also frequently seen at the edges of supergranule cells. The rate of cancellation can be estimated from the recent magnetic carpet model by Parnell (2001) who finds that around 3 to 5 times as many cancellation events occur as emergence events, hence, a reasonable estimate at the rate of cancellation is 3 – 5 per supergranule per day. The rate of occurrence of $n_\lambda = 3$ and $n_p = 3$ blinkers is about $3.2 \times 10^{-22} \text{ cm}^{-2} \text{ s}^{-1}$, or approximately 35 blinkers per supergranule per day. Clearly, both of these types of events occur far too infrequently to account for blinkers. These rates of occurrence suggest that it is not reconnection driven by emergence or cancellation that are causing blinkers, but they do not rule out the possibility that reconnection due to the passing of opposite polarity fragments might be a mechanism. Furthermore, we find that 39% of blinkers do not occur above regions of mixed polarity and that 59% of those lie above regions where one polarity is dominant.

Although our blinkers do not appear to have detectable coronal signatures we can still compare their frequency with that of nanoflares. From the results of Parnell and Jupp (2000) the occurrence rate of nanoflares appears to be between $2.3 \times 10^{-21} \text{ cm}^{-2} \text{ s}^{-1}$ and $7.8 \times 10^{-21} \text{ cm}^{-2} \text{ s}^{-1}$ which is equivalent to around 250 and 850 per supergranule

ule per day. This is significantly greater than the number of blinkers observed.

These results and the fact that blinkers do not appear to have any strong signature in the coronal lines and the ratios of the oxygen species are flat suggests that blinkers are filling factor or density events. Possible mechanisms for blinkers are therefore:

- Iso-thermal compression of pre-existing plasma along fieldlines to increase the density, but not the temperature. Compression that occurs on a longer time-scale than the thermal conduction time-scale along fieldlines could be iso-thermal in nature.
- The gathering together of fieldlines with pre-existing plasma at transition region temperatures to increase the filling factor. Blinkers typically occur above sites of strong magnetic field and so movement of these fields could be achieved by simply moving the other extended footpoints around. Due to the canopy effect any squeezing is likely to effect the chromospheric and transition region plasma more than plasma in widely spaced fieldlines at coronal temperatures. Modelling of the magnetic footpoints below blinkers would help us determine if this mechanism is likely.
- The distant reconnection of fieldlines that extend from a magnetic fragment below the blinker causing them to be ‘slung shot’ over. During a ‘sling shot’ motion fieldlines that start off almost perpendicular to the line of sight, may become parallel to the line-of-sight before ending up perpendicular once more. Although the actual crossing of the fieldlines may happen very fast the time to reconnect all the fieldlines from one fragment may last several minutes and maybe long enough to account for a blinker. Comparing CDS rasters of blinkers and TRACE or Yohkoh images of loops would help decide if this was a likely mechanism.

Recently, a paper by Priest et al. (2001) considered possible mechanisms for blinkers. They mentioned the following mechanisms:

- Spicules: After spicular material reaches coronal heights it may be heated to coronal temperatures before it falls. This falling material may give rise to blinkers. However, there are up to $3.6 \times 10^{-19} \text{ cm}^{-2} \text{ s}^{-1}$ or almost 40,000 per supergranule per day! Priest et al. (2001) suggest that only those effected by granular compression would produce blinkers, but since granulation is occurring at all times it is hard to believe that only 1 in every 1000 is compressed in this way.

- Cool low-lying loops: It is possible for short (5 Mm) loops to remain filled with plasma at temperatures of 10^5 K for several minutes - these could be blinkers. The presence of blinkers above unipolar regions is suggestive of longer fieldlines rather than very short ones. Also considering the size of blinkers many short field lines would be needed which would seem to suggest a fairly obvious opposite polarity fragment should be present.
- Coronal base of hot loops: The movement of the thin layer of plasma at the base of loops that lies between coronal and chromospheric plasma - this could give a blinking effect. This possibility needs to be tested by comparing CDS rasters with TRACE or Yohkoh images of loops.
- Heating and evaporating plasma: Plasma that passes through 10^5 K whilst being heated from chromospheric to coronal temperatures following heating and evaporation may be observed as a blinker. No real consistent flow patterns have been observed in blinkers. This may be because there is no coherent flow in a blinker or just a very weak flow. It is, therefore, hard to say whether things are rising or not. Furthermore, we see no delay in the onset, time of peak or end of a blinker in the different wavelengths. This may be due to the fairly low cadence (3 minutes) in our observations or may be because there is no time lag.
- Cooling and draining plasma: Plasma that is cooling down from coronal to chromospheric temperatures and passing through 10^5 K could also be observed as a blinker. Similar arguments to those above for the heating of plasma apply.

Not only are we unable to distinguish between each of these mechanisms at the moment, but we are also unable to verify if any one is likely to occur.

6. Conclusions

Our results confirm the properties of O V blinkers discovered by Harrison (1997) and Harrison et al. (1999). We find lifetimes from the data resolution up to 40 mins (mean 16 minutes), areas from 1 pixel up to 5.5×10^8 km² (mean approximately 3×10^7 km²) and intensity enhancement ratios of around 1.8. The global frequency is, as expected, much higher at around $1-20$ s⁻¹ depending on whether large or small peak intensities are demanded. The ratios of the oxygen lines are again

shown to be flat confirming the results of Harrison (1997) and Harrison et al. (1999) that blinkers appear to be increases in density or filling factor.

We have investigated the rise and fall times of the O V blinkers. There does not appear to be a clear pattern with 40% having a faster rise than fall time, 40% with a faster fall than rise time and 20% with effectively equal rise and fall times. The mean rise and fall times are both about 8 minutes.

Blinkers that are identified in O V can also be readily detected as blinkers in O IV and He I with 80 – 91% and 23 – 28% of the O V blinkers detected in these lines, respectively. The O IV and He I lines are two of the strongest transition region and chromospheric lines, respectively, that CDS has. In the weaker line, O III, the blinkers are much harder to detect with less than 6% of the O V blinkers seen. The blinkers detected in these wavelengths tend to occur simultaneously with the O V blinkers. No significant peaks at the time of the blinkers are seen in the Mg IX and Mg X coronal lines. In the cases of 4% and 13% of the O V blinkers, small intensity enhancements greater than $n_{\lambda\text{MgIX}} = 1$ and $n_{\lambda\text{MgX}} = 1$ are observed, respectively for the Mg IX and Mg X lines. There are probably more Mg X enhancements of this size because this line has an O IV component. These results suggest that blinkers have no coronal signatures, however, it may be simply that these lines are too weak to detect anything in.

Statistical analysis has been used to confirm that the distribution of blinkers is not uniform and they are preferentially located in regions of strongest emission in the chromospheric and transition region lines studied. This suggests that they are (I) located over the network and that (II) the signatures of blinkers in the He I and oxygen lines are all very similar. The results for the coronal lines suggest that the blinkers occur below regions of medium emission, but not necessary the strongest coronal emission. This result needs further investigation though. For example, a data sequence is needed with longer exposure times so better counts are attained in these lines. Also when analysing these lines it would also be better if each spectrum was first fitted to avoid any affects from the O IV component in the Mg X line.

A statistical analysis was also used to show that the blinkers have a preference for regions with strong absolute magnetic fields. This is of course to be expected since we find 99% of them to occur above the network. However, a rough analysis of the position of blinkers with respect to magnetic fragments show that 88% occur above well defined magnetic fragments. Furthermore, 75% occur above regions where one polarity dominates. These results suggest that local mixed polarity field does not appear to be a key ingredient for blinkers and, hence,

in situ magnetic reconnection may not be the mechanism that causes blinkers. We suggest that an alternative mechanism is the iso-thermal compression of plasma through the movement of magnetic fragments due to granular motions. It is likely that such motions could easily give rise to many small-scale events like the unit brightenings observed in SUMER which could be averaged out to give the CDS blinkers we observe.

Acknowledgements

CDS was built and is operated by a consortium led by the Rutherford Appleton Laboratory and including the Mullard Space Science Laboratory, the NASA Goddard Space Flight Center, Oslo University and the Max-Planck-Institute for Extraterrestrial Physics, Garching. SOHO is a mission of international cooperation between ESA and NASA. DB and CEP would like to thank Alan Hood, Peter Jupp and Dave Pike for their help and useful comments. DB acknowledges support from the Particle Physics and Astronomy Research Council. CEP would like to thank the Royal Astronomical Society for support as the RAS Sir Norman Lockyer Fellow.

References

- Berghmans, D., Clette, F., Moses, D.: 1998, *Astron. Astrophys.* **336**, 1039
 Bewsher, D., Parnell, C.E., Pike, C.D.: 2001, *in preparation*
 Brković, A., Rüedi, I., Solanki, S.K., Fludra, A., Harrison, R.A., Huber, M.C.E., Stenflo, J.O., Stucki, K.: 2000, *Astron. Astrophys.* **353**, 1083
 Brković, A., Solanki, S.K., Rüedi, I.: 2001, *Astron. Astrophys.* **373**, 1056
 Chae, J., Wang, H., Goode, P.R., Fludra, A. and Schühle, U.: 2000, *ApJ* **528**, L119
 Gabriel, A.H.: 1976, *Phil. Trans. R. Soc. Lond. A* **281**, 339
 Gallagher, P.T., Phillips, K.J.H., Harra-Murnion, L.K., Keenan, F.P.: 1999, *Astron. Astrophys.* **335**, 733
 Gallagher, P.T., Phillips, K.J.H., Harra-Murnion, L.K., Baudin, F., Keenan, F.P.: 1999, *Astron. Astrophys.* **348**, 251
 Hagenaar, H.: 2001, *ApJ* **555**, 448.
 Harrison, R.A., Fludra, A., Pike, C.D., Payne, J., Thompson, W.T., Poland, A.I., Breeveld, A.A., Culhane, J.L., Kjeldseth-Moe, O., Huber, M.C.E., Aschenbach, A.: 1995, *Solar Phys.* **162**, 223
 Harrison, R.A.: 1997, *Solar Phys.* **175**, 467.
 Harrison, R.A., Lang, J., Brooks, D.H., Innes, D.E.: 1999, *Astron. Astrophys.* **351**, 1115.
 Parnell, C.E., Jupp, P.E.: 2000, *ApJ* **529**, 554.
 Parnell, C.E.: 2001 *Solar Phys.* in press.

- Priest, E.R., Hood, A.W., Bewsher, D.: 2001, *submitted*
- Scherrer, P.H., Bogart, R.S., Bush, R.I., Hoeksema, J.T., Kosovichev, A.G., Schou, J., Rosenberg, W., Springer, L., Tarbell, T.D., Title, A., Wolfson, C.J., Zayer, I., MDI Engineering Team.: 1995, *Solar Phys.* **162**, 129.
- Teriaca, L., Madjarska, M.S. and Doyle, J.G.: 2001, *Solar Phys.*, in press
- Thompson, W.: 1998, 'Deriving Statistics from NIS Data', *CDS Software Note No.49*

